

Quantum topological Hall effect and noncoplanar antiferromagnetism in $K_{0.5}RhO_2$

Jian Zhou¹, Qi-Feng Liang², Hongming Weng³, Y. B. Chen⁴, Shu-Hua

Yao¹, Yan-Feng Chen^{1,*}, Jinming Dong⁴, and Guang-Yu Guo^{5,6†}

¹ National Laboratory of Solid State Microstructures and Department of Materials Science and Engineering, Nanjing University, Nanjing 210093, China

² Department of Physics, Shaoxing University, Shaoxing 312000, China

³ Beijing National Laboratory for Condensed Matter Physics, and Institute of Physics, Chinese Academy of Sciences, Beijing 100190, China

⁴ National Laboratory of Solid State Microstructures and Department of Physics, Nanjing University, Nanjing 210093, China

⁵ Department of Physics, National Taiwan University, Taipei 10617, Taiwan

⁶ Physics Division, National Center for Theoretical Sciences, Hsinchu 30013, Taiwan

(Dated: March 1, 2016)

Quantum anomalous Hall (QAH) phase is a two-dimensional bulk ferromagnetic insulator with a nonzero Chern number in presence of spin-orbit coupling (SOC) but absence of applied magnetic fields. Associated metallic chiral edge states host dissipationless current transport in electronic devices. This intriguing QAH phase has recently been observed in magnetic impurity-doped topological insulators, *albeit*, at extremely low temperatures. Based on first-principles density functional calculations, here we predict that layered rhodium oxide $K_{0.5}RhO_2$ in noncoplanar chiral antiferromagnetic state is an unconventional three-dimensional QAH insulator with a large band gap and a Neel temperature of a few tens Kelvins. Furthermore, this unconventional QAH phase is revealed to be the exotic quantum topological Hall effect caused by nonzero scalar spin chirality due to the topological spin structure in the system and without the need of net magnetization and SOC.

PACS numbers: 72.15.Gd, 73.43.-f, 75.10.Lp, 75.50.Ee

Introduction. The integer quantum Hall effect (IQHE), first found in 1980 [1], is one of the most important discoveries in condensed matter physics. When a strong perpendicular magnetic field is applied to a two-dimensional (2D) electron gas at low temperatures, the Hall conductance is precisely quantized in units of the fundamental conductance quantum (e^2/h) due to Landau-level quantization. This quantization is subsequently found to be directly connected with the topological property of the 2D bulk insulating states, characterized by a topological invariant called the Chern number [2, 3]. This topological understanding of the IQHE implies that the IQHE can also occur in other time-reversal symmetry (TRS) broken systems with a topological non-trivial band structure in the absence of the external magnetic field and Landau levels, such as a ferromagnetic insulator, leading to the so-called quantum anomalous Hall effect (QAHE). This effect was first proposed by Haldane in a honeycomb lattice model with a staggered magnetic field that produces zero average flux per unit cell [4]. Other model systems have also been proposed including the ferromagnetic quantum wells in the insulating state [5], the disorder-induced Anderson insulator [6], Rashba graphene coupled with exchange field [7, 8], Kagome lattice [9] and ferromagnetic skyrmion crystal [10].

Due to its intriguing nontrivial topological properties and great potential application for designing dissipationless electronics and spintronics, extensive theoretical

studies have been made to search for real materials to host such QAHE. The conventional mechanism for the QAHE is the recognition of the QAHE as the quantized version of the anomalous Hall effect (AHE) in a ferromagnetic metal [11]. In particular, it has been recently established that the Berry curvature in the momentum space caused by the broken TRS due to the magnetization and spin-orbit coupling (SOC), acts as a fictitious magnetic field [12, 13] and thus gives rise to the AHE. In a topologically nontrivial ferromagnetic insulator (Chern insulator), the integral of the Berry curvature over the Brillouin zone (the Berry phase) results in a nonzero Chern number and hence the quantized Hall conductance. [14] Indeed, several *ferromagnetic* insulators are predicted to be the Chern insulators by first-principles band structure calculations based on this mechanism [14, 15]. Importantly, based on the prediction in [15], the QAHE has recently been observed in the Cr-doped $(Bi,Sb)_2Te_3$ ferromagnetic topological insulator films [16]. Nevertheless, the QAH phase appears at extremely low temperatures (less than 30 mK) due to the small band gap (less than 0.01 eV), weak magnetic coupling and low carrier mobility in the sample. This hinders further exploration of the exotic properties of the Chern insulator and also its applications. The low carrier mobility could result from the disorder of the doped magnetic impurities in the sample. Therefore, it would be fruitful to search for the QAHE in crystalline magnetic insulators with a large band gap.

On the other hand, it was found in [9] that in the Kagome lattice, the above-mentioned fictitious magnetic field that gives rise to the AHE, can also be generated by the scalar spin chirality $\kappa = \sum \vec{S}_i \cdot (\vec{S}_j \times \vec{S}_k)$ (where \vec{S}_i, \vec{S}_j

*Corresponding author: yfchen@nju.edu.cn

†Corresponding author: gyguo@phys.ntu.edu.tw

and \vec{S}_k denote three noncoplanar spins in the set) due to the topological nontrivial spin texture in the noncollinear magnetic structure. In such noncoplanar magnetic structure, when an electron moves around a set of three noncoplanar magnetic moments, its wave function would acquire a Berry phase of $\Omega/2$ where Ω is the solid angle subtended by the three magnetic moments. This Berry phase acts as the fictitious magnetic field and generates the AHE even in an antiferromagnet (AFM) without net magnetization. Indeed, this unconventional AHE known as the topological Hall effect (THE) was observed in noncollinear AFMs such as $\text{Nd}_2\text{Mo}_2\text{O}_7$ [17] and $\text{Pr}_2\text{Ir}_2\text{O}_7$ [18]. Nevertheless, the topological Hall conductivity detected in these materials are small, being only a small fraction of the conductance quantum (e^2/h) [17–19].

Here we predict that the easily synthesized layered oxide $\text{K}_{0.5}\text{RhO}_2$ [20, 21] in the noncoplanar antiferromagnetic state (nc-AFM) (Fig. 1) would host the QAH phase with a large band gap of 0.22 eV, based on a systematic first-principles study of its magnetic and electronic properties. We also find that the QAH effect is caused by the nonzero scalar spin chirality in the noncoplanar AFM even in the absence of the SOC and net magnetization, and thus is the quantized THE (QTHE). The calculated exchange coupling parameters between the neighboring Rh atoms reveal that the nc-AFM is caused by the frustrated magnetic interactions in the compound, with an estimated Neel temperature of ~ 20 K. All these findings suggest that the layered $\text{K}_{0.5}\text{RhO}_2$ is a promising candidate of the topological Chern insulator.

Methods. The electronic structure of $\text{K}_{0.5}\text{RhO}_2$ has been calculated based on the density functional theory (DFT) with the generalized gradient approximation (GGA) plus on-site Coulomb repulsion (i.e., the GGA+U scheme) (see [22] for computational details). The experimental lattice constants [23] are used. Nevertheless, the atomic positions are optimized theoretically. [22] Anomalous Hall conductivity (AHC) is calculated by using Wannier interpolation with an effective Hamiltonian constructed in a basis of maximally localized Wannier functions (MLWFs) [24]. The band structure obtained from the effective Hamiltonian agrees well with that from the DFT calculations (see Fig. S3 in [22]).

Noncoplanar antiferromagnetic structure. Layered rhodium oxide K_xRhO_2 has recently received increasing attention [20, 21, 25–27] because it is isostructural and isoelectronic to thermoelectric material Na_xCoO_2 [28]. K_xRhO_2 crystallizes in the $\gamma\text{-Na}_x\text{CoO}_2$ -type structure where the CdI_2 -type RhO_2 layer and the K layer stack alternately along c -axis [20, 21], as illustrated in Fig. 1a. Indeed, significant thermopower and Seebeck coefficient were observed in $\text{K}_{0.49}\text{RhO}_2$ [20] and $\text{K}_{0.63}\text{RhO}_2$ [21], respectively. Furthermore, as for Na_xCoO_2 , K_xRhO_2 could be expected to become superconducting and also exhibit interesting magnetic behaviors at certain potassium concentration (x), which, interestingly, can be tuned by K de-intercalation of KRhO_2 [27]. In particular, Rh atoms in each RhO_2 layer form a two-dimensional triangular

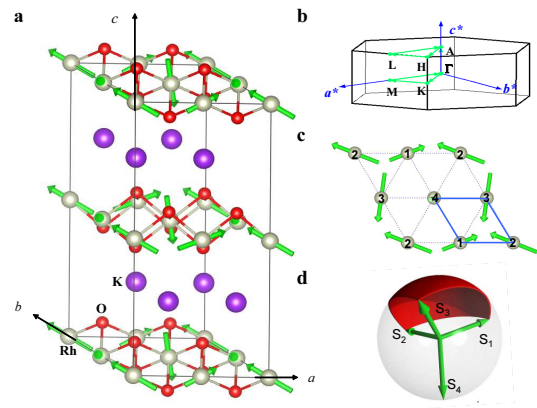


FIG. 1: (Color online) (a) Crystal structure of $\text{K}_{0.5}\text{RhO}_2$ in the $2 \times 2 \times 1$ supercell and (b) its hexagonal Brillouin zone. Green arrows show the Rh magnetic moments in the ground state noncoplanar antiferromagnetic configuration (nc-AFM). (c) Top view of the magnetic structure in one RhO_2 layer. Thin blue lines denote the chemical unit cell. Numbers label the four Rh atoms in the planar supercell. (d) Unit sphere spanned by the four Rh magnetic moments in one RhO_2 layer parallel transported to have a common origin.

lattice which was recently shown to host exotic magnetic states tunable by the band filling factor [29, 30]. In K_xRhO_2 , Rh ions would be Rh^{3+} ($4d^6$) when $x = 1$ and Rh^{4+} ($4d^5$) if $x = 0$. Therefore, Rh atoms in each RhO_2 layer would have their $4d$ orbitals split into partially filled t_{2g} orbitals and empty e_g orbitals [25], and t_{2g} orbitals would be further split into fully occupied double e'_g orbitals and partially occupied single a_{1g} orbital due to the trigonal deformation of RhO_2 octahedra. Interestingly, when $x = 0.5$, Rh ions would be $\text{Rh}^{3.5+}$ ($4d^{5.5}$) and the a_{1g} band would have a filling factor of $3/4$, which was predicted by the mean-field solution of the ferromagnetic Kondo lattice model to have a chiral magnetic ordering and spontaneous quantum Hall effect [29, 30].

Here we investigate the magnetic properties of $\text{K}_{0.5}\text{RhO}_2$ with first-principles DFT calculations. We consider all possible magnetic configurations up to four-sublattice orders on one RhO_2 monolayer (see Figs. S1 and S2 in [22]). We perform total energy calculations for these magnetic configurations within the GGA+U scheme. The calculated total energy and properties of the magnetic structures that could be stabilized during the self-consistent calculations are listed in Table S1 in [22]. It is clear from Table S1 that the all-in/all-out noncollinear nc-AFM configuration (Fig. 1) has the lowest total energy. Furthermore, the nc-AFM configuration is an insulator with a band gap of 0.22 eV, while all the other configurations are metallic.

Quantum topological Hall insulating phase. Plotted in Fig. 2a is the band structure of $\text{K}_{0.5}\text{RhO}_2$ in the nc-AFM configuration. Figure 2a shows that the system is an insulator with a band gap of 0.22 eV. To examine whether the band gap is topologically trivial or not, we

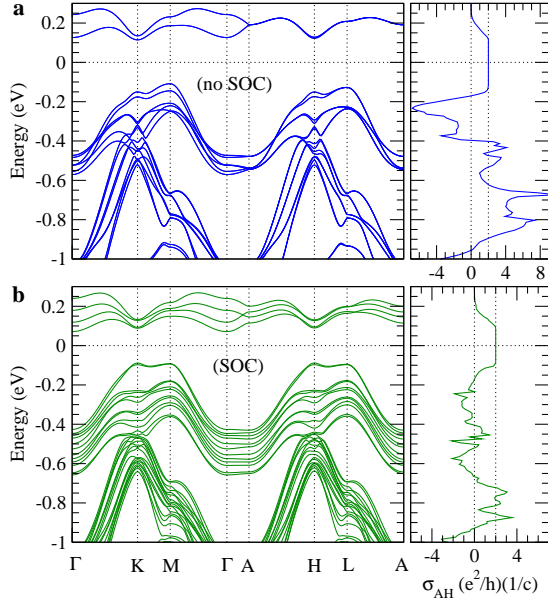


FIG. 2: Band structure and anomalous Hall conductivity (σ_{AH}) of $K_{0.5}RhO_2$ in the noncoplanar antiferromagnetic state (nc-AFM) without SOC (a) and with SOC (b).

further calculate the AHC. For three-dimensional (3D) quantum Hall insulators, AHC $\sigma_{AH} = n e^2/hc$ where c is the lattice constant along c -axis, n should be an integer and equal to the Chern number (n_C) [31]. The calculated AHC is displayed as a function of the Fermi level in Fig. 2a. Indeed, we find that the band gap is topologically nontrivial with the calculated Chern number $n_C = 2.0$, and hence the system is a 3D Chern insulator. Figure 2b shows that the calculated AHC remains constant and equals to $2.0 e^2/hc$ in the entire band gap region.

Since the total magnetization of $K_{0.5}RhO_2$ in the nc-AFM state is zero and the SOC is not included in the electronic structure calculation yet, the obtained nonzero AHC is not caused by spontaneous occurrence of magnetization and SOC[11], and hence is unconventional. Instead, the nonzero AHC results from the nonzero scalar spin chirality $\kappa = \sum \vec{S}_i \cdot (\vec{S}_j \times \vec{S}_k)$ generated by the *noncoplanar chiral* magnetism in the nc-AFM state.[9, 17] In the nc-AFM magnetic configuration, there are four magnetic moments on four Rh atoms in one RhO₂ layer (their unit vectors labelled as S_1, S_2, S_3, S_4 in Fig. 1). By parallel transporting these four unit vectors to have a common origin, we obtain an unit sphere, as shown in Fig. 1d. Therefore, the sum of the four solid angles (Ω) spanned by the four three-spin sets of $\vec{S}_1 \cdot (\vec{S}_2 \times \vec{S}_3)$, $\vec{S}_2 \cdot (\vec{S}_3 \times \vec{S}_4)$, $\vec{S}_3 \cdot (\vec{S}_4 \times \vec{S}_1)$, $\vec{S}_4 \cdot (\vec{S}_1 \times \vec{S}_2)$ is 4π . The associated Berry phase γ is then half of the total solid angle Ω , i.e., $\gamma = \Omega/2 = 2\pi$, and this gives rise to a Chern number of $n_C = \gamma/2\pi = 1$. [14] Since one unit cell contains two RhO₂ layers, the Chern number of the system would be 2 and the AHC $\sigma_{AH} = 2.0 e^2/hc$. Therefore, the QAH insulating phase predicted here is entirely due

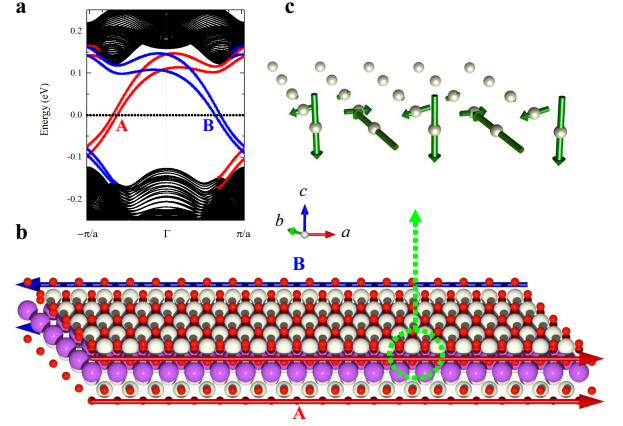


FIG. 3: (a) Band structure of a thick noncoplanar antiferromagnetic $K_{0.5}RhO_2$ ribbon cut along a -axis. Black lines represent projected bulk energy bands, while red (A) and blue (B) lines denote chiral edge states in the bulk band gap on the two opposite sides of the ribbon. In (b), red and blue arrowed lines represent the chiral edge states A and B, respectively, one per RhO₂ layer. (c) Spin texture of the A edge state near the Fermi level in a segment of the $K_{0.5}RhO_2$ ribbon. Green vectors represent the spin moments on the Rh atoms.

to the QTTE. Finally, we note that the sign of the Chern number and AHC could be reversed by reversing all the four magnetic moments, e.g., changing the all-in to all-out nc-AFM configuration (see Fig. S2 in [22]).

Chiral edge states and spin texture. According to the bulk-boundary correspondence[32], the nc-AFM $K_{0.5}RhO_2$ would have one metallic chiral edge state per RhO₂ layer which carries dissipationless charge current. To examine these interesting edge states, we calculate the energy bands for a thick $K_{0.5}RhO_2$ nanoribbon along a -axis using the MLWFs. The thick nanoribbon has a width of 40 unit cells along b -axis and remains periodic along a - and c -axis. The calculated one-dimensional band structure along a -axis is shown in Fig. 3a. We can see that there are four edge states within the bulk band gap, two localized on one edge carrying electrons along positive a direction (red lines) and two sitting on the opposite edge carrying electrons along negative a direction (blue lines). In other words, there are two chiral edge states per unit cell, i.e., one chiral edge state per RhO₂ layer, as illustrated in Fig. 3b. We note that the direction of the dissipationless edge current can be switched by changing the sign of the scalar spin chirality, or by reversing, e.g., the all-in nc-AFM configuration to all-out one.

The spin texture of the edge state in $K_{0.5}RhO_2$ is studied by the one-band tight-binding (TB) Hubbard model analysis (see [22] for details). Figure 3c displays the spin texture of the A edge state near the Fermi level in a segment of the $K_{0.5}RhO_2$ ribbon. We find that the spin moments are well localized on the atoms along the edges and decay rapidly towards the interior of the ribbon.

Discussion. In the above-mentioned electronic struc-

ture calculations, the SOC was not included yet. Therefore, the uncovered quantized AHC can be completely attributed to nonzero scalar spin chirality, and hence results from the genuine QTHE. Nevertheless, the SOC always exists in real materials. In particular, the SOC strength of Rh $4d$ orbitals is not small and hence cannot be ignored. To examine how the electronic structure and especially QTHE discovered here would be affected by the SOC effect, we have repeated the calculations with the SOC included, and the calculated energy bands and AHC are shown in Fig. 2b. It is clear from Fig. 2b that almost all doubly degenerate bands are now split due to the SOC. Figure 2b also indicates that the size of the calculated AHC below the band gap generally gets reduced when compared to Fig. 2a, although the line shape remains similar. Importantly, Fig. 2b shows that the system is still an insulator with a similar band gap (0.16 eV), and also has a quantized AHC with the Chern number of 2. Interestingly, when the SOC is included, the system acquires a small magnetization of $0.08 \mu_B/\text{f.u.}$ due to the spin canting. This small magnetization would provide a coupling between the magnetic structure and external magnetic field and thus allows us to control the sign of the Chern number and the direction of the edge currents by an applied magnetic field.

In order to understand the noncollinear nc-AFM order and also estimate its Neel temperature, we evaluate the exchange coupling parameters between neighboring Rh atoms in one RhO_2 layer by mapping the calculated total energies of the ferromagnetic (FM), striped (s-AFM) and zigzag (z-AFM) antiferromagnetic states (see Table S1 in [22]) to the classical Heisenberg model. In so doing, we obtain the first near-neighbor exchange coupling $J_1 = 4.4 \text{ meV} = 51 \text{ K}$ (FM coupling) and second near-neighbor exchange coupling $J_2 = -3.6 \text{ meV} = -42 \text{ K}$ (AFM coupling). According to the phase diagram of the J_1 - J_2 Heisenberg model [33], this implies that noncollinear magnetic states are energetically favored in $\text{K}_{0.5}\text{RhO}_2$. Furthermore, based on these parameters, a mean-field estimation (see Ref. [34] and references therein) would lead to a Neel temperature of $\sim 20 \text{ K}$ for $\text{K}_{0.5}\text{RhO}_2$, being well above 30 mK at which the QAH effect was observed in thin films of Cr-doped $(\text{Bi,Sb})_2\text{Te}_3$, a ferromagnetic topological insulator [16]. Thus, the QTHE predicted in $\text{K}_{0.5}\text{RhO}_2$ here would provide an easily accessible platform for exploring exotic states of quantum matters and also be promising for technological applications.

To gain detailed insight into the formation of topological insulating gap, we also perform a TB Hamiltonian analysis of the magnetic and electronic properties of one monolayer of $\text{K}_{0.5}\text{RhO}_2$. We consider the one-band TB Hubbard model because the two conduction bands and six top valence bands of $\text{K}_{0.5}\text{RhO}_2$ in the nc-AFM structure (Fig. 2a) are derived mainly from the Rh $4d a_{1g}$ orbital. We solve the model Hamiltonian self-consistently within the mean-field approximation (see [22] for details). We find that the nc-AFM magnetic structure (Fig. 1) is the most stable state, being consistent with the

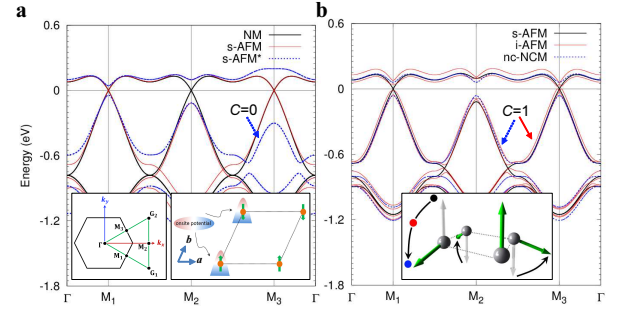


FIG. 4: (a) The TB energy bands of the NM, s-AFM and s-AFM* along the symmetry lines in the Brillouin zone (left inset). The s-AFM* state differs from the s-AFM in that an onsite potential is added on one of the two sites on each ferromagnetic (FM) chain along a -axis (right inset). (b) The TB band structures of the s-AFM and nc-AFM configurations as well as an intermediate noncollinear magnetic state (i-NCM) (inset) which occurs when the s-AFM is transformed to the nc-AFM by spin rotations.

DFT calculations. Figure 4a shows that the TB band structure of the NM state is a metal with conduction and valence bands touching at all three M-points in the BZ at the Fermi level. In the primitive unit cell, the Rh a_{1g} band is $3/4$ -filled and hence metallic. Therefore, in the 2×2 supercell, three of the four a_{1g} bands obtained by folding the energy bands in the primitive unit cell, are completely filled up to the BZ boundary including the M-points. However, the supercell possesses three half-translation symmetries $\mathbf{a}/2$, $\mathbf{b}/2$ or $(\mathbf{a} + \mathbf{b})/2$, and consequently, the conduction and valence bands touch and the bands are doubly degenerate at the M-points. Introducing the striped AFM (s-AFM) (Fig. S1b) configuration breaks the $\mathbf{b}/2$ and $(\mathbf{a} + \mathbf{b})/2$ half-translation symmetries, although preserves the half-translation $\mathbf{a}/2$, and thus opens a gap at the M₂-point in the BZ. Putting an extra onsite potential on two sites in the supercell (see the right inset in Fig. 4a) further lifts the $\mathbf{a}/2$ half-translation symmetry and opens a gap at the M₁ and M₃ points. Therefore, the resultant AFM* state is an insulator. Nevertheless, it is not a QAH insulator because the calculated Chern number $n_C = 0$.

Similarly, the nc-AFM configuration also breaks the three half-translation symmetries and thus opens a gap at all three M-points (Fig. 4b). In contrast, however, the gap is nontrivial because the calculated $n_C = 1$. Note that the nc-AFM configuration can be obtained from the s-AFM state by rotating the spins on the four sublattices (see the inset in Fig. 4b). Interestingly, all these intermediate states are a QAH insulating state with $n_C = 1$, except the s-AFM state where the Chern number is ill-defined because it is a metal. This is caused by the fact that all the intermediate states have a nonzero scalar spin chirality with total solid angle spanned by the four spins is 4π , as for the nc-AFM state. These results clearly demonstrate that the QAH phase found here is robust

against variation of the magnetic structure around the nc-AFM.

As mentioned before, the nc-AFM order was recently predicted in the ferromagnetic Kondo triangular lattice model due to the perfect Fermi surface nesting at the $3/4$ band filling [29, 30]. As found here, the nc-AFM phase is insulating and exhibits spontaneous quantum Hall effect [29, 30]. Thus, given the well known predictive power of the DFT calculations, the QAH phase discovered here in $K_{0.5}RhO_2$ is a materialization of the prediction of the QTHE in the ferromagnetic Kondo triangular lattice model [29, 30], *albeit*, with a distinct origin. We also notice that Hamamoto *et al.* very recently predicted the QTHE in the skyrmion crystal based on the double-exchange model calculations [10]. In this model, the conduction electrons are assumed to strongly couple to the background skyrmion spin texture and thus acquire a Berry phase when they hop among the non-collinear spin moments. Therefore, the mechanism is the

same as that in the ferromagnetic Kondo lattice model in which the noncollinear local spin moments of the magnetic ions, instead of the skyrmions, provide the fictitious magnetic field and Berry phase. However, the QTHE in the skyrmion crystal [10] differs in several significant ways from the one predicted in the present paper. For example, a strong SOC (e.g., Dzyaloshinskii-Moriya interaction or Rashba interaction) is needed to stabilize the skyrmion crystal [10]. Furthermore, a skyrmion crystal is formed in a ferromagnet.

This work is supported by the State Key Program for Basic Research (2015CB659400 and 2013CB632700), the National Science Foundation of China (Nos. 11474150, 11574215, 11274359, and 11422428) and the Scientific Research Foundation for the Returned Overseas Chinese Scholars, Ministry of Education of China as well as the Ministry of Science and Technology, National Center for Theoretical Sciences and Academia Sinica in Taiwan. J.Z. and Q.F.L. contributed equally to this work.

-
- [1] K. V. Klitzing, G. Dorda, and M. Pepper, Phys. Rev. Lett. **45**, 494 (1980).
 - [2] D. J. Thouless, M. Kohmoto, M. P. Nightingale, and M. den Nijs, Phys. Rev. Lett. **49**, 405 (1982).
 - [3] R. B. Laughlin, Phys. Rev. Lett. **50**, 1395 (1983).
 - [4] F. D. M. Haldane, Phys. Rev. Lett. **61**, 2015 (1988).
 - [5] C. X. Liu, X.-L. Qi, X. Dai, Z. Fang and S.-C. Zhang, Phys. Rev. Lett. **101**, 146802 (2008).
 - [6] M. Onoda and N. Nagaosa, Phys. Rev. Lett. **90**, 206601 (2003).
 - [7] Z. H. Qiao, S. A. Yang, W. X. Feng, W.-K. Tse, J. Ding, Y. G. Yao, J. Wang and Q. Niu, Phys. Rev. B **82**, 161414(R) (2010).
 - [8] T.-W. Chen, Z.-R. Xiao, D.-W. Chiou and G. Y. Guo, Phys. Rev. B **84**, 165453 (2011).
 - [9] K. Ohgushi, S. Murakami and N. Nagaosa, Phys. Rev. B **62**, 6065 (2000).
 - [10] K. Hamamoto, M. Ezawa, and N. Nagaosa, Phys. Rev. B **92**, 115417 (2015).
 - [11] N. Nagaosa, J. Sinova, S. Onoda, A. H. MacDonald, and N. P. Ong, Rev. Mod. Phys. **82**, 1539 (2010).
 - [12] Z. Fang, N. Nagaosa, K. S. Takahashi, A. Asamitsu, R. Mathieu, T. Ogasawara, H. Yamada, M. Kawasaki, Y. Tokura, and K. Terakura, Science **302**, 92 (2003).
 - [13] D. Xiao, M.-C. Chang and Q. Niu, Rev. Mod. Phys. **82**, 1959 (2010).
 - [14] H. M. Weng, R. Yu, X. Hu, X. Dai, and Z. Fang, Advances in Physics, **64**, 227 (2015).
 - [15] R. Yu, W. Zhang, H. J. Zhang, S. C. Zhang, X. Dai, and Z. Fang, Science **329**, 61 (2010).
 - [16] C.-Z. Chang, J. Zhang, X. Feng, J. Shen, Z. Zhang, M. Guo, K. Li, Y. Ou, P. Wei, L.-L. Wang, Z.-Q. Ji, Y. Feng, S. Ji, X. Chen, J. Jia, X. Dai, Z. Fang, S.-C. Zhang, K. He, Y. Wang, L. Lu, X.-C. Ma, Q.-K. Xue, Science **340**, 167 (2013).
 - [17] Y. Taguchi, Y. Oohara, H. Yoshizawa, N. Nagaosa, and Y. Tokura, Science, **291**, 2573 (2001).
 - [18] Y. Machida, S. Nakatsuji, S. Onoda, T. Tayama, and T. Sakakibara, Nature, **463**, 210 (2008).
 - [19] C. Sürgers, G. Fischer, P. Winkel and H. v. Löhneysen, Nature Commun. **5**, 3400 (2014).
 - [20] S. Shibusaki, Y. Nishina, I. Terasaki, K. Yubuta, and T. Kajitani, J. Phys.: Condens. Matter. **22**, 115603 (2010).
 - [21] S. H. Yao, B. B. Zhang, J. Zhou, Y. B. Chen, S. T. Zhang, Z. B. Gu, S. T. Dong, and Y. F. Chen, AIP Advances **2**, 042140 (2012).
 - [22] See Supplemental Materials at <http://link.aps.org/supplemental/> for details.
 - [23] K. Yubuta, S. Shibusaki, I. Terasaki, and T. Kajitani, Philosophical Magazine, **89**, 2813 (2009).
 - [24] A. A. Mostofi, J. R. Yates, Y.-S. Lee, I. Souza, D. Vanderbilt and N. Marzari, Comput. Phys. Commun. **178**, 685 (2008).
 - [25] R. Okazaki, Y. Nishina, Y. Yasui, S. Shibusaki, and I. Terasaki, Phys. Rev. B **84**, 075110 (2011).
 - [26] Y. Saeed, N. Singh, and U. Schwingenschlogl, Adv. Func. Mater. **22**, 2792 (2012).
 - [27] B. B. Zhang, S. T. Dong, Y. B. Chen, L. Y. Zhang, J. Zhou, S. H. Yao, Z. B. Gu, S. T. Zhang, and Y. F. Chen, Cryst. Eng. Comm. **15**, 5050 (2013).
 - [28] R. Schaak, T. Klimczuk, M. L. Foo, and R. J. Cava, Nature **424**, 527 (2003).
 - [29] I. Martin and C. D. Batista, Phys. Rev. Lett. **101**, 156402 (2008).
 - [30] Y. Akagi and Y. Motome, J. Phys. Soc. Japan, **79**, 083711 (2010).
 - [31] B. I. Halperin, Jpn. J. Appl. Suppl. **26**, 1913 (1987).
 - [32] A. M. Essin, and V. Gurarie, Phys. Rev. B **84**, 125132 (2011).
 - [33] S. N. Saadatmand, B. J. Powell and I. P. McCulloch, Phys. Rev. B **91**, 245119 (2015).
 - [34] J. C. Tung and G. Y. Guo, Phys. Rev. B **83**, 144403 (2011).